HHS Public Access

Author manuscript

Mol Cell. Author manuscript; available in PMC 2022 December 16.

Published in final edited form as:

Mol Cell. 2021 December 16; 81(24): 5052–5065.e6. doi:10.1016/j.molcel.2021.10.028.

HRD1-mediated METTL14 degradation regulates m^{6}A mRNA modification to suppress ER proteotoxic liver disease

Juncheng Wei[1,8], **Bryan T. Harada**[2,3], **Dan Lu**[4], **Ruihua Ma**[5], **Beixue Gao**[1], **Yanan Xu**[1], **Elena Montauti**[1], **Nikita Mani**[1], **Shuvam Chaudhuri**[1], **Shana Gregory**[1], **Samuel Weinberg**[1], **Donna Zhang**[6], **Richard Green**[7], **Chuan He**[2,3], **Deyu Fang**[1,8,9]

[1]Department of Pathology, Northwestern University Feinberg School of Medicine, Chicago, IL, 60611, USA

[2]Department of Chemistry and Department of Biochemistry and Molecular Biology, The University of Chicago, Chicago, IL 60637, USA.

[3]Howard Hughes Medical Institute, The University of Chicago, Chicago, IL 60637, USA.

[4]Department of Molecular Biosciences, Northwestern University, Evanston, IL 60208, USA

[5]Division of Pulmonary and Critical Care Medicine, Department of Medicine, Northwestern University Feinberg School of Medicine, Chicago, IL, USA.

[6]Department of Pharmacology and Toxicology, College of Pharmacy, University of Arizona, Tucson, Arizona 85721, USA

[7]Division of Gastroenterology and Hepatology, Department of Medicine, Northwestern University Feinberg School of Medicine, Chicago, IL, 60611, USA

Summary

Accumulation of unfolded or misfolded proteins in the endoplasmic reticulum (ER) lumen triggers unfolded protein response (UPR) for stress adaptation, the failure of which induces cell apoptosis and tissue/organ damage. The molecular switches underlying how the UPR selects for stress adaptation over apoptosis remain unknown. Here we discovered that accumulation of unfolded/misfolded proteins selectively induces N^6-adenosine-methyltransferase-14 (METTL14) expression. METTL14 promotes CHOP mRNA decay through its 3'UTR N^6-adenosine methylation (m^{6}A) to inhibit its downstream proapoptotic target genes expression. UPR induces METTL14 expression through competing the HRD1-ERAD machinery to block METTL14 ubiquitination and degradation. Therefore, mice with liver-specific METTL14 deletion are highly

[8]Correspondence should be addressed to J.W (Juncheng.wei@northwestern.edu) and D.F. (fangd@northwestern.edu).
[9]Lead Contact: Deyu Fang (fangd@northwestern.edu)

Author contributions: JW, BH, DL, RM, BG, YX, EM, NM, SC, DZ, SG, and SW performed the experiments and analyzed the data. RG and JW contributed critical reagent and in experimental design. JW, CH and DF designed the study, analyzed the data, and wrote the manuscript.

Disclosure of Conflicts of Interest: C.H. is a scientific founder and a member of the scientific advisory board of Accent Therapeutics, Inc. All other authors declare no competing financial interests.

susceptible to both acute pharmacological and alpha-1 antitrypsin (AAT) deficiency-induced ER proteotoxic stress and liver injury. Further hepatic CHOP deletion protects METTL14 knockout mice from ER stress-induced liver damage. Our study reveals a crosstalk between ER stress and mRNA m^6A pathways, the ERm^6A pathway, for ER stress adaptation to proteotoxicity.

Graphical Abstract

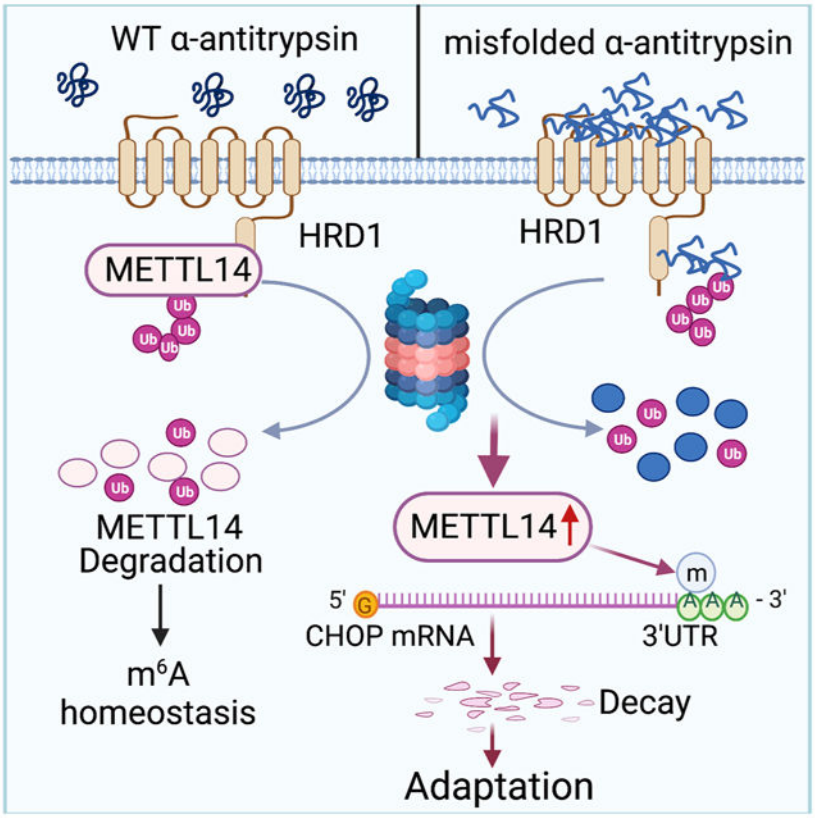

Lay summary:

Alpha-1 antitrypsin deficiency (AATD) is a common inherited cause of liver disease with the most severe mutation found in 1:3500 live births and currently 180,000 individuals worldwide. The disease is caused by the accumulation of a misfolded AAT-Z protein in hepatocytes' ER lumen, leading to inflammation, fibrosis, cirrhosis, and increased risk of hepatocellular carcinoma. Clinical studies have suggested that a substantial amount of AATD infants do not develop liver toxicity, in which the hepatocytes often express low levels of CHOP, a transcription factor that promotes ER stress-induced apoptosis, implying a possibility that their hepatocytes adapt to misfolded protein induced toxicity through CHOP suppression. However, the molecular mechanisms underlying how CHOP expression is controlled during ER stress remain largely unknown. Here we have discovered that misfolded AAT-Z protein accumulation in hepatocytes in PiZ mice induces METTL14 expression that catalyzes CHOP mRNA methylation, which promotes its decay and consequently suppresses CHOP protein expression. At the molecular level, the misfolded proteins compete with METTL14 for HRD1, an enzyme that ubiquitinates METTL14 for degradation. Our study reveals a previously unappreciated molecular switch

in regulating misfolded protein induced liver toxicity and provides a rationale for potential manipulation of HRD1-METTL14 crosstalk in AATD therapy.

eTOC Blurb

ERAD is critical for ER-stress adaptation, and its failure triggers cell apoptosis. Wei et al discovered that ER-stress induces the N^6-adenosine-methyltransferase METTL14 expression by suppressing HRD1-mediated ubiquitination to promote CHOP mRNA decay for inhibiting CHOP-induced apoptosis. This study defines an ERm^6A pathway underlying how ERAD selects stress adaptation over apoptosis.

INTRODUCTION

The endoplasmic reticulum (ER) is a dynamic and multifunctional organelle responsible for the biosynthesis, folding, assembly, modification and quality control of secretory and membrane proteins (Hetz et al., 2020; Wang and Kaufman, 2016). Impairment in the ability to handle protein folding and proteostasis disrupts ER homeostasis and results in the aggregation of misfolded proteins in different cellular compartments, which are hallmarks of various human diseases, including Alzheimer's disease and α1-antitrypsin (AAT) deficiency (Berg and Eriksson, 1972; Schröder and Kaufman, 2005; Wang and Kaufman, 2016). Misfolded proteins within the ER lumen usually trigger adaptive measures termed as the unfolded protein response (UPR) through three canonical pathways: the Protein kinase R-like ER kinase (PERK)-eukaryotic translation initiation factor 2α (eIF2α) pathway (which attenuates global mRNA translation), and the Cyclic AMP-dependent transcription factor 6 (ATF6) pathway and the Inositol-requiring transmembrane kinase/endoribonuclease 1α (IRE1α)- X-box-binding protein 1s(−Xbp1s) pathway (both of which induce transcription of genes involved in protein folding and degradation) (Hetz et al., 2019; Samuel and Shulman, 2012). In contrast, if the adaptive response fails, apoptotic cell death ensues through activation of the pro-apoptotic Cyclic AMP-dependent transcription factor 4 (ATF4) -CHOP pathway (Wei and Fang, 2021).

AAT deficiency is a genetic disease caused by mutation of the serine protease inhibitor 1A (SERPINA1) gene (Strnad et al., 2020). This mutation results in a toxic misfolded protein that is prone to polymerization and accumulation in the lumen of ER of hepatocytes (Stoller and Aboussouan, 2012; Strnad et al., 2020). The misfolded AAT-Z protein forms aggregated polymers that are retained within the ER of hepatocytes and leads to liver damages. Recent studies have indicated that C/EBP-homologous protein (CHOP), a transcription factor promotes ER stress-induced apoptosis, was found among the most up-regulated genes in livers of PiZ mice and in human livers of patients homozygous for the Z allele (Attanasio et al., 2020; Pastore et al., 2017), implying a pathogenic role of CHOP in AAT deficiency. Clinical surveys have also observed that AAT-Z protein accumulation could only induce minimal increase in CHOP protein expression in a some individuals with SERPINA1 mutation (Attanasio et al., 2020; Ponzetto et al., 2017). Therefore, those infants with homozygous AATD are asymptomatic and clinically recover in early childhood. However, how CHOP expression is regulated during AATD induced pathogenesis remains mysterious.

N^6-methyladenosine (m^6A) is the most common mRNA modification and has been shown to regulate mRNA translation, decay, splicing, and nuclear export (Liu et al., 2020; Shi et al., 2019; Yue et al., 2015). The m^6A is regulated by m^6A "writers" (METTL3/METTL14 complex), "readers" (YTHDF1-3), and "erasers" (FTO and ALKBH5) (He and He, 2021). This system has shown to be induced by extracellular stimulation, such as heat shock or infection, to modulate numerous processes including cell differentiation, innate immune response and apoptosis in diverse organisms (Chen et al., 2019; Frye et al., 2018; Patil et al., 2018; Wang and He, 2014; Wang et al., 2017). However, the molecular mechanisms underlying how the m^6A process is regulated by extra- and intra- cellular pathophysiological responses, such as ER stress and UPR, remain largely unclear.

HMG-CoA reductase degradation protein 1 (HRD1) is an E3 ligase for degradation of unfolded/misfolded proteins in the ER, a process referred to as ER-associated degradation (ERAD) (Christianson and Ye, 2014; Kikkert et al., 2004; Shimizu et al., 2010). The HRD1-ERAD machinery has been shown to recognize the Z variant of SERPINA1/AAT aggregation and promote its ubiquitination and degradation to protect the liver from AATD (Karatas and Bouchecareilh, 2020). In addition to unfolded protein substrates, HRD1 catalyzes ubiquitin-conjugation of the canonical ER stress modulator IRE1α, which is negatively regulated by unfolded protein accumulation and ER stress response(Gao et al., 2008; Sun et al., 2015). Recently, we found that HRD1 targets multiple metabolic enzymes to maintain hepatic and whole-body energy homeostasis (Chen et al., 2020; Kim et al., 2021; Wei et al., 2018a; Wei et al., 2018b). Intriguingly, loss of HRD1 in dendritic cells diminishes MHC-II expression and protects mice from experimental autoimmune encephalomyelitis (Yang et al., 2014). In contrast, HRD1 fine-tunes T cell immune homeostasis through promoting T cell activation and Treg stabilization (Xu et al., 2019; Xu et al., 2016) . These findings point to a cell type-specific effect of HRD1, as well as the significance of specific substrates in mediating the effects of ERAD *in vivo*.

Here we discovered METTL14 as a regulator of ER proteotoxic stress adaptation. ER proteotoxic stress upregulates METTL14 expression and the targeted hepatic deletion of METTL14 sensitizes mice to misfolded protein-induced liver damage. Interestingly, while METTL14 is a substrate for HRD1, misfolded proteins outcompete METTL14 as HRD1 substrates during UPR, leading to upregulation of METTL14, which suppresses CHOP protein expression through m^6A mRNA modification. Therefore, the switch of HRD1 from degrading METTL14 to degrading misfolded proteins when misfolded/unfolded proteins accumulate is a key event regulating cellular adaptation to ER stress.

RESULTS

Unfolded protein accumulation and ER proteotoxic stress upregulate METTL14.

To investigate the possible crosstalk between m^6A mRNA modification with ER stress, we analyzed the expression of m^6A "writer" proteins METTL3 and METTL14 and "eraser" protein ALKBH5 *in vivo* and *in vitro* upon ER stress activation. The m^6A writer protein METTL14, but not METTL3, was dramatically increased by pharmacologic induction of ER stress with tunicamycin (Tm) in HepG2 human hepatoma cells (Figure 1A). Similarly, the m^6A writer protein METTL14, but not METTL3, was selectively upregulated in liver tissues

from mice treated with Tm (2 mg/kg, i.p.) (Figure 1B). In contrast, the m^{6}A eraser ALKBH5 protein expression was not altered by Tm-induced ER stress *in vivo* and *in vitro* (Figures 1A and 1B). Further, immunofluorescence (IF) staining confirmed the specific increase in hepatic METTL14 expression (Figures 1C and S1A). Of note, while METTL14 is mainly localized to the nucleus under normal condition, Tm stimulation resulted in a significant METTL14 increase in both cytoplasm and nuclear (Figure 1C). METTL14 protein elevation could be detected 16 hours after Tm stimulation (Figure 1D). The abundance of global mRNA m^{6}A modification was increased in liver cells after Tm treatment, consistent with greater METTL14 activity (Figure S1B), confirming that pharmacological induction of ER stress promotes METTL14 protein expression and function.

Mice with a transgenic expression of the human AAT variant, PiZ, in the livers cause an ER accumulation of unfolded human AAT and ATTD-like pathogenesis (Carlson et al., 1989). We found that the m^{6}A writer protein METTL14, but not METTL3, was dramatically increased in the livers of the PiZ mice (Figure 1E). In contrast, the protein expression of the m^{6}A eraser ALKBH5 was not affected by transgenic AAT expression in mice (Figure 1E). Similar to the gradual accumulation observed during pharmacological ER stress, METTL14 upregulation was detected in liver from the age of 6 weeks and further increased at 8-12 weeks (Figure 1F). However, this METTL14 protein increase was not detected in the liver tissues of PiZ mice at the age of 2 weeks, when the AAT protein aggregation was often undetectable in their liver (Figure 1F). Our results indicate that UPR selectively induces the m^{6}A writer METTL14 expression in liver cells.

METTL14 protects against ER stress-induced liver injury.

To examine the functional consequence of ER stress-induced METTL14 expression, we crossed METTL14 floxed (METTL14$^{f/f}$) mice with mice harboring a Cre transgene under the control of the albumin promoter (Alb-Cre$^+$), and generated liver-specific METTL14 conditional knockout (METTL14$^{f/f}$Alb-Cre$^+$; METTL14^{Alb}) mice (Figure S2A). A complete deletion of METTL14 mRNA was confirmed in the liver of METTL14 ^{Alb} mice (Figure S2B). METTL14^{Alb} mice were normal in appearance and behavior with comparable body weight and without any detectable liver toxicities because the liver enzyme alanine transaminase (ALT) was unaltered (Figures S2C-S2E). However, when challenged with pharmacologic ER stress inducer tunicamycin, all of the *METTL14^{Alb}* mice died within 4 days. In contrast, all WT mice survived after treated with the same dose of Tm (Figure 2A). Tm treatment significantly reduced the body weight in *METTL14^{Alb}* mice, but with a much smaller effect on the control *METTL14$^{f/f}$Alb-Cre$^-$* WT mice (Figure 2B). Compared with their WT littermates, *METTL14^{Alb}* mice developed hepatomegaly upon Tm challenge (Figures 2C and 2D). Liver panel tests showed that serum markers of liver damage including ALT and alkaline phosphatase (ALP), but not blood urea nitrogen (BUN), were significantly increased in the *METTL14^{Alb}* mice (Figure 2E). Hematoxylin and eosin (H&E) stain confirmed more hepatocyte necrosis and hepatocyte number reduction in the *METTL14^{Alb}* mice (Figures 2F and 2G). These results indicate that hepatic METTL14 plays an essential role in protecting mice from the pharmacological ER stress-induced liver injury.

METT14-mediated m^{6}A modification inhibits CHOP expression.

To investigate the molecular mechanisms underlying how METTL14 protects mice from UPR-induced liver damage, we analyzed the mRNA expression profile in liver from Tm treated METTL14 LKO and WT mice. Under ER stress condition, 1,802 genes were decreased by more than 50% and 2,131 genes were increased for at least 2-fold in liver by METTL14 deletion (Figures 2H and S3A). Functional analysis identified the top pathways of the upregulated genes by METTL14 deletion include cytoskeleton organization, cell cycle, ER stress-mediated activation of MAPK and NF-kB, O-linked glycosylation and apoptosis (Figures S3A and S3B). In contrast, downregulated genes are involved in metabolic regulation, peroxisome and fatty acid oxidation (Figure S3A), indicating that METTL14 is involved in a variety of critical biological functions in liver. Interestingly, the proapoptotic CHOP gene and its downstream target targets, *Abcc4, Ndrg1, Atf3, Gadd34a* and *Slc4a11*, were increased in *METTL14*^{Alb} livers under Tm stimulation (Figures 2H and 2K). The qPCR and western blotting analysis further confirmed CHOP upregulation in *METTL14*^{Alb} livers (Figures 2I and 2J), but ATF4 protein levels were unaltered (Figure 2I). Consistently, Gene Set Enrichment Analysis (GSEA) showed that CHOP targets were enriched in the genes upregulated in Tm-treated *METTL14*^{Alb} livers (Figure S3C), indicating METTL14-deficeicy induces liver damage through, at least partially, activating the CHOP proapoptotic pathway.

As a critical m^{6}A modification writer, METTL14 may regulate CHOP expression through m^{6}A methylation of CHOP mRNA. To test this, we preformed m^{6}A-IP-RT-qPCR to quantify relative *Chop* mRNA m^{6}A levels by immunoprecipitation with m^{6}A-specific antibody. Figure S3D showed that *Chop* mRNA m^{6}A modification was dramatically increased upon Tm stimulation, possibly due to the upregulated METTL14 protein expression. Indeed, targeted METTL14 deletion resulted in a dramatic reduction in the m^{6}A mRNA modification on CHOP 3'UTR in *METTL14*^{Alb} livers (Figure 2L).

We then used the CRISPR-mediated METTL14 gene deletion to further validate whether METTL14 regulates CHOP protein abundance *in vitro*. Indeed, CHOP protein was dramatically increased by the METTL14 gene deletion (Figure 2M). Consistent to our notion that METTL14-deletion caused liver damage during ER stress (Figures 2E and 2G), the viability and CHOP mRNA of the METTL14 KO NIH3T3 cells was also decreased upon Tm stimulation (Figure S3E). Interestingly, CHOP mRNA was more stable in the METTL14 KO NIH3T3 cells (Figure 2N). Bioinformatics prediction showed that there are five potential m^{6}A sites in the 3'UTR of *Chop* mRNA (Figure 2O). Interestingly, mutation of these five m^{6}A sites dramatically increased *Chop* mRNA stability (Figure 2O), indicating that METT14 suppresses CHOP expression through its 3'UTR m^{6}A modification-mediated mRNA decay. Collectively, our data reveal that METTL14 down-regulates CHOP protein expression through m^{6}A methylation-mediated mRNA degradation to protect cells from ER stress-induced apoptosis.

METTL14 ablation aggravates chronic proteotoxic stress induced liver damage.

To further investigate the role of METTL14 in chronic proteotoxic stress induced liver damage, we crossed METTL14^{Alb} mice with PiZ mice, whose liver express the

mutant human AT-Z gene that leads to an accumulation of misfolded Z alpha-antitrypsin (Carlson et al., 1989). PiZ mice grow normally, and the gross morphology of their livers appeared similar to that of WT littermates (Figures 3A-3C). In contrast, liver-specific METTL14 deletion significantly enhanced the Z alpha-antitrypsin induced pathogenesis with 70% of the PiZ/METTL14^{Alb} mice died by the age of 15 weeks (Figure 3A). While the PiZ/METTL14^{Alb} mice were born normally, their body weights and heights were dramatically decreased comparing to their PiZ/METTL14$^{f/f}$ littermates (Figures 3B and 3D). METTL14^{Alb}/PiZ mice developed typical cirrhosis symptoms with visible nodules and fibrosis in their shrunken livers (Figure 3C). The levels of ALT and ALP as well as bile acids were dramatically increased in the serum of METTL14^{Alb} PiZ mice (Figure 3E). Histological analysis showed extensive round cytoplasmic globules with extensive portal tract fibrosis in the liver tissues from METTL14^{Alb}/PiZ mice (Figure 3F). Sirius red staining detected a dramatic accumulation in collagen deposition in the Piz/METTL14^{Alb} livers as compared with Piz/METTL14$^{f/f}$ livers (Figure 3F). These results indicate that METTL14 deletion facilitates misfolded protein Z alpha-antitrypsin-induced liver damage. Consistent with what we observed in pharmacological ER stress models, CHOP expression was also dramatically increased in the Piz/METTL14^{Alb} livers (Figure 3G). As a consequence, the expression of CHOP target genes *Atf3* and *Gadd34, Bak1* and *Bax* were increased in Piz/METTL14^{Alb} livers (Figure 3H). Collectively, these results imply that METTL14 protects misfolded protein Z alpha-antitrypsin-induced liver damage through, at least partially, suppressing CHOP protein expression.

ER proteotoxic stress upregulates METTL14 through suppressing its ubiquitination-mediated degradation by HRD1.

To determine the molecular mechanisms underlying how ER proteotoxic stress regulates METTL14 protein expression, we first asked whether METTL14 is upregulated at mRNA level. However, the mRNA levels of METTL14, as well as METTL3, were unaltered by Tm treatment (Figure 4A). In contrast, mRNA levels of a well-known ER stress target gene X-box binding protein 1 Spliced (Xbp1s) were increased upon ER stress activation by Tm (Figures 4A and S4A), indicating that ER stress induces METTL14 at the post-transcriptional level. ATF4 mRNA translation is regulated by upstream open read frames (ORFs) under ER stress activation (Vattem and Wek, 2004), implying a possibility that METTL14 protein expression could be regulated similarly. However, unlike ATF4, bioinformatics analysis did not detect any uORFs in the 5′ noncoding region of the METTL14 mRNA and the translational efficiency of METTL14 mRNA was comparable between Tm treated and control HepG2 cells (Figures S4B and S4C). Interestingly, while METTL14 protein was gradually degraded in HepG2 cells, Tm treatment largely protected METTL14 from degradation, pointing to a possibility that ER stress inhibits METTL14 protein turnover (Figure 4B). Indeed, Tm treatment gradually inhibited METTL14, but not METTL3, ubiquitination over time (Figures 4C and S4D), indicating that ER stress upregulates METTL14 through suppressing its ubiquitination-mediated protein degradation. This conclusion was further confirmed *in vivo* because unfolded human AAT accumulation with age in PiZ mouse liver dramatically inhibited METTL14 ubiquitination without affecting it mRNA expression (Figures 4D and 4E). Of note, unfolded AAT accumulation reversibly correlated to METTL14 ubiquitination (Figure 4F), but positively correlated to

METTL14 protein expression in livers of PiZ mice with age (Figure 4E). Collectively, these results indicated that UPR upregulates METTL14 protein expression through suppressing its ubiquitination-mediated degradation (Figure 4G).

Next, we investigated whether HRD1 is an E3 ubiquitin ligase of METTL14. Co-immunoprecipitation (IP) and immunoblotting analysis detected HRD1 interaction with METTL14, but not METTL3, in transiently transfected HEK293 cells (Figure 5A). In addition, HRD1 could endogenously interact with METTL14 (Figure 5B). The methyltransferase domain (EPPL and SAM binding domain) of METTL14, which mediated its dimerization with METTL3 and mRNA recruitment, is sufficient for its interaction with HRD1 (Figure 5C). The HRD1 protein contains six transmembrane domains and its cytoplasmic tail carries an E3 ligase catalytic RING finger and a long proline-rich C terminus (Figure 5D). However, deletion of the transmembrane domains in HRD1 did not affect its interaction with METTL14 (Figure 5D), indicating that the RING finger-containing cytoplasmic domain of HRD1 (HRD1-C) is involved in METTL14 interaction.

Importantly, HRD1 overexpression dramatically increased METTL14 ubiquitination (Figure 5E), while mutation of the critical cysteine in the RING-finger of HRD1 prevented the increase in METTL14 ubiquitination (Figure 5E). In addition, expression of and HRD1-C, which mediated the METTL14 interaction, expression was sufficient to promote METTL14 ubiquitination (Figure 5F). Conversely, HRD1 deletion in HepG2 cells decreased the endogenous ubiquitination of METTL14 (Figure 5G). Importantly, the misfolded, but not wild-type AAT, expression dramatically inhibited HRD1-induced METTL14 ubiquitination (Figures 5H and S5A), clearly indicating that the misfolded proteins compete HRD1 with METTL14 for ubiquitination. Consistent to our observation that the misfolded AAT expression is reversely associated to METTL14 ubiquitination (Figures 4E and 4F), the ubiquitination of METTL14 was dramatically inhibited by pharmacological UPR inducer Tm (Figure 5I). To support this, HRD1 deletion dramatically prolonged the half-life of METTL14 protein in liver cells (Figures 5J and S5B). In contrast, the half-life of METTL3 was unaltered by HRD1 deletion (Figure S5B). Collectively, these results indicate that HRD1 is an E3 ubiquitin ligase of METTL14, and ER proteotoxic stress upregulates METTL14 through suppressing HRD1-mediated METTL14 ubiquitination.

The ER resident E3 ubiquitin ligase HRD1 controls METTL14 protein expression.

Next, we validated whether METTL14 protein level is regulated by HRD1 ERAD pathway *in vivo*. Indeed, an about 10 to 15-fold increase in METTL14 protein expression levels was detected in liver and primary hepatocytes lacking the ERAD-associated E3 ubiquitin-protein ligase HRD1 (Figures 6A and 6D). In contrast, the protein expression levels of another m^6A writer METTL3, as well as the m^6A erasers ALKBH5 and FTO were unaltered by HRD1 ablation (Figure 6A and 6D). Global mRNA m^6A levels were increased in HRD1 ablation livers (Figure S6A). Notably, *Chop* m^6A mRNA modification were greatly increased in Piz transgenic and HRD1 ablation livers (Figure S6B). Immunofluorescence staining confirmed the increase in METTL14 in both nuclear and cytoplasm in HRD1-null hepatocytes (Figure 6B). HRD1-deficiency upregulates METTL14 protein expression at post-transcriptional levels because its knockout had no effect on hepatic METTL14 mRNA

transcription (Figure 6C). To further investigate the roles of METTL14 elevation in HRD1 liver specific KO mice, we generated liver-specific METTL14/HRD1 double knockout mice. As we previously reported (Wei et al., 2018a), HRD1 deletion didn't result in severe liver toxicity (Figures S6C and S6D). In contrast, liver-specific METTL14 deletion in $HRD1^{Alb}$ mice significantly enhanced HRD1 deletion induced hepatic pathogenesis with 80% of the $HRD1^{Alb}METTL14^{Alb}$ mice dying by the age of 12 weeks (Figure S6C). The body weights of $HRD1^{Alb}METTL14^{Alb}$ mice were decreased comparing to their $HRD1^{Alb}$ littermates (Figure S6D). The levels of ALT and ALP were dramatically increased in the serum of $HRD1^{Alb}METTL14^{Alb}$ mice (Figure S6E). Collectively, these results imply that METTL14 serve as master regulator to protect HRD1 deletion induced liver damage (Figure S6F).

Liver specific HRD1 KO mice have profound metabolic changes with lower body weight or growth retardation (Wei et al., 2018a), raising a concern that the increase in METTL14 proteins in HRD1-null liver could be an indirect effect. We then generated a strain $Mx1\text{-}Cre^{+}$ $HRD1^{flox/flox}$ mice with inducible HRD1 deletion by polyI:C injection. As shown in Figure 6E, 4 days after poly I:C treatment, METTL14 was dramatically increased in the liver by polyI:C-induced HRD1 deletion, but no change in body weights could be detected. Similarly, METTL14 was also accumulated in the bone marrow after polyI:C treatment, indicating that HRD1 is a critical regulator of METTL14 protein stability in multiple tissues/organs (Figure 6F). Importantly, in contrast to the fact that Tm upregulated METTL14 protein expression in the liver of WT mice, Tm treatment failed to further induce METTL14 elevation in the $Hrd1^{-/-}$ livers, indicating ER stress induces METTL14 expression in a HRD1-dependent manner (Figure 6G).

METTL14 protects AAZ-induced liver injury through suppressing CHOP protein expression.

Our data thus far have suggested that ER proteotoxic stress upregulates METTL14 to inhibit the proapoptotic CHOP protein expression and protects cells from ER proteotoxic stress. To further determine the role of CHOP in METTL14 protective functions, we generated liver specific METTL14/CHOP double knockout ($METTL14^{Alb}CHOP^{Alb}$) PiZ mice. The deletion of CHOP protein expression in liver tissues from $METTL14^{Alb}CHOP^{Alb}$ PiZ mice confirmed by western blotting (Figure 7A). As previously published (Attanasio et al., 2020), $Piz/CHOP^{f/f}$ and $Piz/CHOP^{Alb}$ mice grow normally (Figure S7A) with normal serum ALP and ALT levels (Figure S7B). H&E staining did not detect any histological abnormalities in the liver of $Piz/CHOP^{f/f}$ & $Piz/CHOP^{Alb}$ mice (Figure S7C). Importantly, while METTL14 deficiency resulted in the death of PiZ mice (Figures 3A and 7B), further hepatic CHOP deletion fully protected $METTL14^{Alb}$ PiZ mice from liver damage-induced death (Figure 7B), indicating a dominant role of CHOP in liver pathogenesis caused by METTL14 deficiency. To support this notion, we further observed that hepatic CHOP deletion restored the growth retardation of $METTL14^{Alb}$ PiZ mice (Figures 7C and 7D). Liver morphological analysis show that CHOP deletion largely diminished the cirrhosis symptoms including visible nodules and shrunken livers in $METTL14^{Alb}$ PiZ mice (Figure 7E). Also, the serum levels of ALT, ALP, bile acids and bilirubin, which were dramatically increased in of $METTL14^{Alb}$ PiZ mice, were restored back to nearly normal by further CHOP deletion (Figure 7F). In addition, histological analysis confirmed the protective roles

of CHOP deletion in liver damage in METTL14^{Alb} PiZ mice (Figure 7G). Collectively, our data demonstrated that the METTL14-deficiency failed to protect UPR-mediated cell proteotoxicity largely due to the increase in CHOP protein expression. Therefore, METTL14 plays a critical role in cell adaptation to UPR-induced cell toxicity through suppressing the expression of the pro-apoptotic factor CHOP (Figure 7H).

DISCUSSION

The endoplasmic reticulum (ER) is a dynamic and multifunctional organelle responsible for protein biosynthesis, folding, assembly, and modification (Walter and Ron, 2011; Wang and Kaufman, 2016). Impairment in the ability of the cell to handle protein folding and proteostasis disrupts ER homeostasis and leads to the accumulation of unfolded and misfolded proteins and ER stress (Hetz et al., 2019; Samuel and Shulman, 2012). Chronic ER stress is hepatotoxic and contributes to the development of chronic liver diseases (Bozaykut et al., 2016; Cubillos-Ruiz et al., 2017; Lebeaupin et al., 2018). AAT deficiency is a classic example and common inherited cause of liver disease with the most severe mutation found in approximately 1 in 2,000-5,000 births and currently 180,000 individuals worldwide (Karatas and Bouchecareilh, 2020; Strnad et al., 2020). Interestingly, among PiZZ children, the presentation of the liver disease can be highly variable. The majority of AAT deficient children recover clinically through unknown molecular mechanisms (Feldman and Sokol, 2013). We show here that the misfolded protein accumulation induces METTL14 protein expression to protect UPR-induced proteotoxicity. Upregulation of METTL14 suppresses the pro-apoptotic transcription factor CHOP expression through m^{6}A modification of its mRNA. It has been well-established that to adapt the unfolded protein accumulation and ER stress, the cell will attenuate global mRNA translation (Guan et al., 2014). The m^{6}A modification of mRNA governs a general and widespread link between transcription and translation upon different extracellular stress including heat shock, ultraviolet and virus infection (Price et al., 2020; Xiang et al., 2017; Zhou et al., 2015). Therefore, our studies have identified a previously unknown molecular mechanism that adapts the cellular response to ER stress, the ER stress-m^{6}A pathway or ERm^{6}A in response to misfolded/unfolded protein accumulation. It will be interesting to elucidate whether dysregulation in m^{6}A modification machinery is responsible for the frailer in adaptation to AAT-induced ER stress in patients.

HRD1 is involved in the degradation of unfolded/misfolded proteins in the ER, a process referred to as ER-associated degradation (ERAD) (Christianson and Ye, 2014; Kikkert et al., 2004; Shimizu et al., 2010). Recently, we and other labs revealed that HRD1 targets other proteins to maintain homeostasis in various organs (Bhattacharya et al., 2018; Hwang and Qi, 2018; Shi et al., 2017; Wei et al., 2018a; Wei et al., 2018b; Xu et al., 2016; Yang et al., 2018).

Our current studies demonstrated that UPR selectively upregulates the m^{6}A writer METTL14 though suppressing HRD1-mediated METTL14 ubiquitination and degradation. In contrast, METTL3 ubiquitination was unaltered by pharmacological UPR-inducer. As a ER transmembrane protein, HRD1 is known to target several nuclear proteins through binding them either in the cytoplasm or in the inner-nuclear membrane via ER nuclear

membrane fusion (Koch and Yu, 2019). Similarly, we have recently demonstrated that HRD1-ERAD promotes the ubiquitination and degradation under basal conditions in a BiP-dependent manner, which is attenuated by accumulation of misfolded/unfolded proteins (Sun et al., 2015). To our knowledge, HRD1 is the first E3 ubiquitin ligase identified that regulates m^6A modification process through targeting METTL14 for degradation. Therefore, HRD1 is a dominant negative regulator of m^6A mRNA modification and thus plays a role in cellular adaptation to ER stress via the ERm^6A mechanism.

Our study shows that CHOP appears to be one of the critical downstream targets for the ERAD-m^6A adaptation pathway during ER stress. Targeted deletion of METTL14 results in elevated CHOP expression and CHOP deletion largely rescues proteotoxicity in METTL14-null liver. METTL14 appears to suppress CHOP expression through m6A methylation of the mRNA 3UTR and consequently triggers CHOP mRNA degradation. CHOP has been recently found as one of the most up-regulated genes in livers of PiZ mice and in young human patients homozygous for the Z allele (Ponzetto et al., 2017). Targeted deletion of CHOP significantly reduced misfolded AAT expression in PiZ mice (Attanasio et al., 2020). It has been well established that the expression of CHOP is rapidly induced by PERK-ATF4 pathway. This study reveals an additional possible molecular mechanism underlying how CHOP expression is upregulated during PiZ pathogenesis through suppressing METTL14-mediated m^6A modification of CHOP mRNA. In addition to CHOP, transcription factors including ATF6 and Xbp-1 play critical role in ER proteotoxic stress response (Kelly et al., 2009; Smith et al., 2011; Van't Wout et al., 2015). Future studies are needed to identify additional downstream target of METTL14 in ER stress adaptation and their involvement in proteotoxicity-induced diseases including alpha 1-antitrypsin induced liver disease.

Limitations of study

The present study reveals that CHOP deletion largely rescued METTL14-deletion induced liner damage in PiZ mice, indicating that METTL14-mediated CHOP suppression is a critical molecular mechanism for liver cell ER stress adaptation when unfolded/misfolded proteins accumulate in the ER. However, in addition to CHOP and its target genes, the expression levels of a variety of genes were altered in hepatocytes by METTL14 deletion. Future studies are needed to identify additional downstream targets of METTL14 in ER stress adaptation and their involvement in proteotoxicity-induced diseases including alpha 1-antitrypsin induced liver disease. In addition, AATD is a common inherited cause of liver disease, with the most severe mutation found in 1:3500 live births and currently 180,000 individuals worldwide. The disease is caused by the accumulation of a misfolded AAT-Z protein in hepatocytes' ER lumen, leading to inflammation, fibrosis, cirrhosis, and increased risk of hepatocellular carcinoma. Clinical surveys have also observed that AAT-Z protein accumulation could only induce minimal increase in CHOP protein expression in some individuals with SERPINA1 mutation. As a consequence, those infants with homozygous AATD are asymptomatic and clinically recover in early childhood. It will be interesting to directly analyze whether METTL14 is differentially expressed in sick and asymptomatic kids with AATD. However, it has been technically challenging to obtain liver biopsies because only extremely limited needle biopsies are collected for sick AATD infants, and liver biopsies are never collected from asymptomatic individuals even with AATD.

STAR ★METHODS

RESOURCEAVAILABILITY

Lead Contact: Further information and requests for resources and reagents should be directed to and will be fulfilled by the Lead Contact Deyu Fang (fangd@northwestern.edu)

Materials availability: All plasmids and mice generated in this study are available from the Lead Contact without restriction.

Data and code availability:

- RNA-seq data have been deposited at GEO and can be accessed at (https://www.ncbi.nlm.nih.gov/geo/query/acc.cgi?acc=GSE185109). Accession numbers are listed in the key resources table.
- Original western blot images and Microscopy data have been deposited at Mendeley (https://data.mendeley.com/datasets/cnn3hhztjm/draft?a=2dc0af50-0cb8-437e-babl-fe23fa5e57a6) and are publicly available as of the date of publication. The DOI is listed in the key resources table.
- This study did not report original code.
- Any additional information required to reanalyze the data reported in this paper is available from the lead contact upon request.

EXPERIMENTAL MODEL AND SUBJECT DETAILS

Mice.—METTL14 floxed and HRD1 floxed mice were used as previously described (Weng et al., 2018; Yang et al., 2014). Breeding of heterozygous mice yielded HRD1$^{flox/flox}$ mice and METTL14$^{flox/flox}$ mice without phenotypic abnormalities in expected Mendelian ratios. Mxl-Cre (catalog no. 003556), CHOP floxed (catalog no. 030816) and Albumin-Cre mice (catalog no. 016832) are at the C57BL/6 genetic background and purchased from The Jackson Laboratory. NSG-PiZ mice (catalog no. 028842) are purchased from Jackson Laboratory and backcrossed to C57BL/6 genetic background. All mice were bred in a specific pathogen-free facility, and all animal experiments were approved by the institutional animal care and use committees (IACUC) at Northwestern University. Animals were maintained on a standard chow diet under 12-hour light and dark cycles beginning at 5:00 a.m. and 5:00 p.m., respectively.

Plasmids, antibodies and other reagents.—The full-length and truncation mutants of HRD1, HA-Ubiquitin expression plasmid, Flag-METTL14 expression were used as reported previously (Kong et al., 2016; Yang et al., 2014). Myc-METTL14 was constructed to pCMV-Myc (Clontech, CA, USA) as reported before (Kong et al., 2016; Yang et al., 2014). The truncation mutants of both HRD1 and METTL14 were generated by PCR and subcloned into pCMV-Flag (Sigma-Aldrich) or pCMV-Myc vectors (Clontech, CA, USA). Antibodies to Flag (F-1804), Anti-Actin (A2103), Anti-HRD1 (HPA024300) were purchased from Sigma (St. Louis, MO, USA), and antibodies to Myc (sc-40), Myc-HRP (sc-40-HRP) and HA-HRP (sc-7392), Anti-GFP (sc-8334) were purchased from Santa Cruz (Santa Cruz, CA, USA). Anti-METTL14 (ab98166), anti-METTL3 (ab195352), anti-

FTO (ab124892) and anti-ALKBH5 (ab195377) anti-human AAT (EPR17087-50) were purchased from Abcam (Cambridge, MA, USA). Anti-GAPDH (2118S), Anti-Ubiquitin (3933S), Anti-CHOP (5554S) were purchased from Cell Signaling Technology (Danvers, MA, USA). Tunicamycin was purchase from Tocris. Poly I:C, Actinomycin D and cycloheximide (CHX) were purchase from Sigma (St. Louis, MO, USA)

METHOD DETAILS

Serum liver function test.—Alkaline Phosphatase (ALP), Alanine Aminotransferase (ALT), bile acid and total bilirubin levels were determined using a chemistry analyzer, VetScan VS2 (Abaxis North America) and the VetScan prep profile II rotor by the Northwestern University Comprehensive Transplant Center Microsurgery Core.

Cell culture, transfection, immunoprecipitation and Western Blot.—HEK293 cells and HepG2 cells were cultured in Dulbecco's Modified Eagle Medium (DMEM) supplemented with 10% fetal bovine serum. Transfections were performed with Lipofectamine 3000 (L3000150, Invitrogen, Carlsbad, CA) according to the manufacturer's instructions. HEK293 cells were transfected with the indicated expression vectors. After 48 h, the cells were lysed in RIPA lysis buffer supplemented with protease (Roche, Basel, Switzerland) and phosphatase inhibitor cocktails. The cell lysates were precleared for 3 times, 15 min each time, with 50 ml Sepharose beads. Co-immunoprecipitation and immunoblotting analyses were performed as described previously (Wei et al., 2014; Wei et al., 2012; Xu et al., 2016). The chemiluminescent blots were imaged with ChemiDoc MP imaging system (Bio-Rad). The Band Analysis tools of ImageLab software version 4.1 (Bio-Rad) were used to select and determine the background-subtracted density of the bands in all the blots. For background subtraction, a value of 1 was used while imaging the blot images for the total protein measurements from the lanes, while for imager data acquired from the chemiluminescent blots, a rolling disc between 10 and 25 was used to ensure a consistent peak cutting for densitometric analysis.

Primary hepatocyte isolation and culture.—To isolate murine primary hepatocytes, livers of 16 weeks old mice were first perfused by HBSS supplemented with 8 mM HEPES (pH 7.35) and 1mM sodium pyruvate followed by collagenase type 1 (Worthington Biochemical Corporation) digestion. Hepatocytes were pelleted by centrifugation at 50g for 2 min, washed three times with DMEM media, and then seeded in the collagen-coated plates with Williams E media.

Translating Ribosome Affinity Purification (TRAP).—Briefly, HepG2 cells were transfected with pSicoR-eIF1a-GFP-RPL10a. 48 hours after transfection, the cells were stimulated with Tm (1ug/ml) for 8 hours. 10min before cell harvest, 100 μg/mL of CHX was added in culture media for 10 min. Cells were homogenized in ice-cold lysis buffer (20 mM HEPES, 5 mM MgCl2, 150 mM KCl, 1% NP-40, 0.5 mM DTT, 100 mg/ml cyclohexamide, RNase inhibitors and protease inhibitors) by passing through pre-chilled 23- then 25-gauge needles 10× each. Separate 10% of the lysate for input of the qPCR and 90% of samples centrifuged at 2,000 x g for 10 min to remove large debris. Supernatants were incubated with streptavidin/protein G-coated Dynabeads (New England Biolabs) bound to anti-GFP

antibodies for 1 hours at 4 °C with gentle mixing. Anti-GFP beads were washed with high salt buffer (20 mM HEPES, 5 mM MgCl2, 350 mM KCl, 1% NP-40, 0.5 mM DTT and 100 mg/ml cyclohexamide) and RNA was eluted from all samples using RNeasy Kits (Qiagen) according to the manufacturer's instructions. RNA yield was quantified using RiboGreen (Life Technologies) and RNA quality was determined by Bioanalyzer analysis.

RNA purification.—Total RNA was purified with TRIzol reagents (Thermofisher Scientific, #15596018) from liver tissues and Rneasy mini kit (QIAGEN, #74106) from cells. Polyadenylated RNA was purified from total RNA with polyA tail purification using GenElute mRNA kits (Sigma, # MRN10).

The m^{6}A RNA immunoprecipitation, transcriptome-wide sequencing and real-time quantitative RT-PCR.—WT and METTL14^{Alb} mice were i.p injected with Tm (2mg/kg) for 24 hours. For transcriptome-wide RNA sequencing, total hepatic RNA was isolated with TRIzol reagent. Polyadenylated RNA was enriched using a Dynabeads mRNA purification kit (Sigma, #MRN10). The mRNA was fragmented using a Bioruptor ultrasonicator (Diagenode) with 30s on/off for 30 cycles. m^{6}A-IP was performed using the Epimark N^6-methyladenosine enrichment kit (New England Biolabs) and library preparation was performed using the Illumina TruSeq Stranded mRNA Sample Prep Kit according to previously published protocols(Dominissini et al., 2012). Two samples were prepared for each condition, and sequencing was carried out at the University of Chicago Genomics Facility on an Illumina HiSeq4000 machine in single-read mode with 50 base pairs per read. HISAT2 (version 2.1.0) was used to align the sequence reads to reference genome and transcriptome (mm10) (Kim et al., 2015). The m^{6}A peaks identification and differential methylation analysis were performed using MeRIPtools (Zhang et al., 2019). Differential gene expression was calculated using DESeq2 (version 1.18.1) using the sequencing reads from input samples (Love et al., 2014). GO Term enrichment analysis was performed using PANTHER (Mi et al., 2013), and Gene Set Enrichment Analysis was performed using GSEA software created by Broad Institute (Subramanian et al., 2005).

Immunofluorescence.—Adult livers were isolated from mice perfused with 4% PFA, and post-fixed in 4% PFA at 4°C for 5 hours. Livers were then immersed in 30% sucrose overnight at 4°C, embedded in Tissue-Tek and cryosectioned (10 μm). Sections were incubated in blocking solution (Roche 11096176001, Mannheim, Germany) at room temperature for 30 min, then incubated with primary antibodies at room temperature overnight and with secondary antibodies for 2 hours at room temperature. Signals were developed with fluorescent-conjugated secondary antibodies and nuclei were stained with DAPI (Cell Signaling Technology). Immunostaining images were obtained with a ZEISS Axioscop 2 fluorescence microscope and processed with Adobe 520 Photoshop CC (Adobe Systems).

QUANTIFICATION AND STATISTIC ALANALYSIS

Quantification of RNA m^{6}A modification levels via mass spectrometry.—Total RNA was purified with TRIZOL reagent then subjected to two rounds of poly(A) selection with the Dynabeads mRNA purification kit (Invitrogen). 25 ng of the purified mRNA was

digested by nuclease P1 (1 U) in 20 μl of buffer containing 20 mM NH4OAc pH 5.5 at 42 °C for 2 h, followed by the addition FastAP buffer (2.3μL, Thermo Scientific) and alkaline phosphatase (1 U) and incubation at 37 °C for 4 h. The sample was then filtered (0.22 μm pore size, 4 mm diameter, Millipore), and 5 μl of the solution was injected into the LC-MS/MS. The nucleosides were separated by reverse-phase ultra-performance liquid chromatography on a C18 column (Agilent) with online mass spectrometry detection using a Sciex 6500+ triple-quadrupole LC mass spectrometer in positive electrospray ionization mode. The nucleosides were quantified by using the nucleoside-to-base ion mass transitions of 282 to 150 (m^6A) and 268 to 136 (A). Quantification was carried out by comparison with a standard curve obtained from pure nucleoside standards run with the same batch of samples. The ratio of m^6A to A was calculated based on the calibrated concentrations.

Quantitative PCR.—The qPCR was run on a Bio-Rad IQ2 PCR machine, and each PCR mixture contained 40 ng of cDNA template and 10 nM primers in 15 μl of SYBR green reaction mix (QuantaBio). The Expression values were normalized to those that were obtained with the control *actb* (encoding beta-actin). Expression was measured using the primers as mentioned previously (Wei et al., 2014), and changes in gene expression levels were calculated by the $2^{-\Delta\Delta Ct}$ method (Wei et al., 2014).

Statistical analyses.—Comparisons between groups were made by unpaired two-tailed Student's *t* test unless otherwise indicated. Survival curves were compared by the Log-rank (Mantel-Cox) test. $P < 0.05$ was considered statistically significant. Statistical analyses were performed using GraphPad Prism (GraphPad Software Inc.). Data are expressed as the mean ± SEM.

Supplementary Material

Refer to Web version on PubMed Central for supplementary material.

ACKNOWLEDGMENTS

This work was supported by the National Institutes of Health (NIH) R21 grant (HD104904) and funded in part by a grant from the alpha-1 foundation to J.W, NIH R01 grants (CA257520, CA232347, DK120330 and DK126908) to D.F. NIHR35ES031575 to D. Z., NIHR01DK093807 & DK121997 to R.G., and RM1 HG008935 to C.H. B.T.H was supported by a National Cancer Institute F32 fellowship (CA221007). C.H. is a Howard Hughes Medical Institute Investigator.

REFERENCES

Attanasio S, Ferriero R, Gernoux G, De Cegli R, Carissimo A, Nusco E, Campione S, Teckman J, Mueller C, Piccolo P, et al. (2020). CHOP and c-JUN up-regulate the mutant Z α(1)-antitrypsin, exacerbating its aggregation and liver proteotoxicity. The Journal of biological chemistry 295, 13213–13223. [PubMed: 32723872]

Berg NO, and Eriksson S (1972). Liver disease in adults with alpha-1 -antitrypsin deficiency. The New England journal of medicine 287, 1264–1267. [PubMed: 4117996]

Bhattacharya A, Sun S, Wang H, Liu M, Long Q, Yin L, Kersten S, Zhang K, and Qi L (2018). Hepatic Sel1L-Hrd1 ER-associated degradation (ERAD) manages FGF21 levels and systemic metabolism via CREBH. The EMBO journal 37.

Bozaykut P, Sahin A, Karademir B, and Ozer NK (2016). Endoplasmic reticulum stress related molecular mechanisms in nonalcoholic steatohepatitis. Mechanisms of ageing and development 157, 17–29. [PubMed: 27393639]

Carlson JA, Rogers BB, Sifers RN, Finegold MJ, Clift SM, DeMayo FJ, Bullock DW, and Woo SL (1989). Accumulation of PiZ alpha 1-antitrypsin causes liver damage in transgenic mice. The Journal of clinical investigation 83, 1183–1190. [PubMed: 2784798]

Chen L, Wei J, Zhu H, Pan H, and Fang D (2020). Energy supplementation rescues growth restriction and female infertility of mice with hepatic HRD1 ablation. American journal of translational research 12, 2018–2027. [PubMed: 32509196]

Chen YG, Chen R, Ahmad S, Verma R, Kasturi SP, Amaya L, Broughton JP, Kim J, Cadena C, Pulendran B, et al. (2019). N6-Methyladenosine Modification Controls Circular RNA Immunity. Molecular cell 76, 96–109.el09. [PubMed: 31474572]

Christianson JC, and Ye Y (2014). Cleaning up in the endoplasmic reticulum: ubiquitin in charge. Nature structural & molecular biology 21, 325–335.

Cubillos-Ruiz JR, Bettigole SE, and Glimcher LH (2017). Tumorigenic and Immunosuppressive Effects of Endoplasmic Reticulum Stress in Cancer. Cell 168, 692–706. [PubMed: 28187289]

Dominissini D, Moshitch-Moshkovitz S, Schwartz S, Salmon-Divon M, Ungar L, Osenberg S, Cesarkas K, Jacob-Hirsch J, Amariglio N, Kupiec M, et al. (2012). Topology of the human and mouse m6A RNA methylomes revealed by m6A-seq. Nature 485, 201–206. [PubMed: 22575960]

Feldman A, and Sokol RJ (2013). Alpha-1-Antitrypsin Deficiency: An Important Cause of Pediatric Liver Disease. Lung health professional magazine 4, 8–11. [PubMed: 27019872]

Frye M, Harada BT, Behm M, and He C (2018). RNA modifications modulate gene expression during development. Science (New York, N.Y.) 361, 1346–1349.

Gao B, Lee SM, Chen A, Zhang J, Zhang DD, Kannan K, Ortmann RA, and Fang D (2008). Synoviolin promotes IRE1 ubiquitination and degradation in synovial fibroblasts from mice with collagen-induced arthritis. EMBO reports 9, 480–485. [PubMed: 18369366]

Guan BJ, Krokowski D, Majumder M, Schmotzer CL, Kimball SR, Merrick WC, Koromilas AE, and Hatzoglou M (2014). Translational control during endoplasmic reticulum stress beyond phosphorylation of the translation initiation factor eIF2α. The Journal of biological chemistry 289, 12593–12611. [PubMed: 24648524]

He PC, and He C (2021). m(6) A RNA methylation: from mechanisms to therapeutic potential. The EMBO journal 40, e105977. [PubMed: 33470439]

Hetz C, Axten JM, and Patterson JB (2019). Pharmacological targeting of the unfolded protein response for disease intervention. Nature chemical biology 15, 764–775. [PubMed: 31320759]

Hetz C, Zhang K, and Kaufman RJ (2020). Mechanisms, regulation and functions of the unfolded protein response. Nature reviews. Molecular cell biology 21, 421–438. [PubMed: 32457508]

Hwang J, and Qi L (2018). Quality Control in the Endoplasmic Reticulum: Crosstalk between ERAD and UPR pathways. Trends in biochemical sciences 43, 593–605. [PubMed: 30056836]

Karatas E, and Bouchecareilh M (2020). Alpha 1-Antitrypsin Deficiency: A Disorder of Proteostasis-Mediated Protein Folding and Trafficking Pathways. International journal of molecular sciences 21.

Kelly E, Greene CM, Carroll TP, McElvaney NG, and O'Neill SJ (2009). Selenoprotein S/SEPS1 modifies endoplasmic reticulum stress in Z variant alpha1-antitrypsin deficiency. The Journal of biological chemistry 284, 16891–16897. [PubMed: 19398551]

Kikkert M, Doolman R, Dai M, Avner R, Hassink G, van Voorden S, Thanedar S, Roitelman J, Chau V, and Wiertz E (2004). Human HRD1 is an E3 ubiquitin ligase involved in degradation of proteins from the endoplasmic reticulum. J Biol Chem 279, 3525–3534. [PubMed: 14593114]

Kim D, Langmead B, and Salzberg SL (2015). HISAT: a fast spliced aligner with low memory requirements. Nature methods 12, 357–360. [PubMed: 25751142]

Kim H, Wei J, Song Z, Mottillo E, Samavati L, Zhang R, Li L, Chen X, Jena BP, Lin JD, et al. (2021). Regulation of hepatic circadian metabolism by the E3 ubiquitin ligase HRD1-controlled CREBH/PPARα transcriptional program. Molecular metabolism 49, 101192. [PubMed: 33592335]

Koch B, and Yu HG (2019). Regulation of inner nuclear membrane associated protein degradation. Nucleus 10, 169–180. [PubMed: 31313624]

Kong S, Yang Y, Xu Y, Wang Y, Zhang Y, Melo-Cardenas J, Xu X, Gao B, Thorp EB, Zhang DD, et al. (2016). Endoplasmic reticulum-resident E3 ubiquitin ligase Hrd1 controls B-cell immunity through degradation of the death receptor CD95/Fas. Proc Natl Acad Sci U S A 113, 10394–10399. [PubMed: 27573825]

Lebeaupin C, Vallée D, Hazari Y, Hetz C, Chevet E, and Bailly-Maitre B (2018). Endoplasmic reticulum stress signalling and the pathogenesis of non-alcoholic fatty liver disease. Journal of hepatology 69, 927–947. [PubMed: 29940269]

Liu J, Li K, Cai J, Zhang M, Zhang X, Xiong X, Meng H, Xu X, Huang Z, Peng J, et al. (2020). Landscape and Regulation of m(6)A and m(6)Am Methylome across Human and Mouse Tissues. Molecular cell 77, 426–440.e426. [PubMed: 31676230]

Love MI, Huber W, and Anders S (2014). Moderated estimation of fold change and dispersion for RNA-seq data with DESeq2. Genome biology 15, 550. [PubMed: 25516281]

Mi H, Muruganujan A, and Thomas PD (2013). PANTHER in 2013: modeling the evolution of gene function, and other gene attributes, in the context of phylogenetic trees. Nucleic acids research 41, D377–386. [PubMed: 23193289]

Pastore N, Attanasio S, Granese B, Castello R, Teckman J, Wilson AA, Ballabio A, and Brunetti-Pierri N (2017). Activation of the c-Jun N-terminal kinase pathway aggravates proteotoxicity of hepatic mutant Z alpha1-antitrypsin. Hepatology (Baltimore, Md.) 65, 1865–1874.

Patil DP, Pickering BF, and Jaffrey SR (2018). Reading m(6)A in the Transcriptome: m(6)A-Binding Proteins. Trends in cell biology 28, 113–127. [PubMed: 29103884]

Ponzetto A, Perez-Perez GI, and Figura N (2017). Alpha1-antitrypsin deficiency and c-JUN. Hepatology (Baltimore, Md.) 66, 677.

Price AM, Hayer KE, McIntyre ABR, Gokhale NS, Abebe JS, Della Fera AN, Mason CE, Horner SM, Wilson AC, Depledge DP, et al. (2020). Direct RNA sequencing reveals m(6)A modifications on adenovirus RNA are necessary for efficient splicing. Nature communications 11, 6016.

Samuel VT, and Shulman GI (2012). Mechanisms for insulin resistance: common threads and missing links. Cell 148, 852–871. [PubMed: 22385956]

Schröder M, and Kaufman RJ (2005). ER stress and the unfolded protein response. Mutation research 569, 29–63. [PubMed: 15603751]

Shi G, Somlo DRM, Kim GH, Prescianotto-Baschong C, Sun S, Beuret N, Long Q, Rutishauser J, Arvan P, Spiess M, et al. (2017). ER-associated degradation is required for vasopressin prohormone processing and systemic water homeostasis. The Journal of clinical investigation 127, 3897–3912. [PubMed: 28920920]

Shi H, Wei J, and He C (2019). Where, When, and How: Context-Dependent Functions of RNA Methylation Writers, Readers, and Erasers. Molecular cell 74, 640–650. [PubMed: 31100245]

Shimizu Y, Okuda-Shimizu Y, and Hendershot LM (2010). Ubiquitylation of an ERAD substrate occurs on multiple types of amino acids. Molecular cell 40, 917–926. [PubMed: 21172657]

Smith SE, Granell S, Salcedo-Sicilia L, Baldini G, Egea G, Teckman JH, and Baldini G (2011). Activating transcription factor 6 limits intracellular accumulation of mutant α(1)-antitrypsin Z and mitochondrial damage in hepatoma cells. The Journal of biological chemistry 286, 41563–41577. [PubMed: 21976666]

Stoller JK, and Aboussouan LS (2012). A review of α1-antitrypsin deficiency. American journal of respiratory and critical care medicine 185, 246–259. [PubMed: 21960536]

Strnad P, McElvaney NG, and Lomas DA (2020). Alpha(1)-Antitrypsin Deficiency. The New England journal of medicine 382, 1443–1455. [PubMed: 32268028]

Subramanian A, Tamayo P, Mootha VK, Mukherjee S, Ebert BL, Gillette MA, Paulovich A, Pomeroy SL, Golub TR, Lander ES, et al. (2005). Gene set enrichment analysis: a knowledge-based approach for interpreting genome-wide expression profiles. Proceedings of the National Academy of Sciences of the United States of America 102, 15545–15550. [PubMed: 16199517]

Sun S, Shi G, Sha H, Ji Y, Han X, Shu X, Ma H, Inoue T, Gao B, Kim H, et al. (2015). IRE1α is an endogenous substrate of endoplasmic-reticulum-associated degradation. Nature cell biology 17, 1546–1555. [PubMed: 26551274]

Van't Wout EF, van Schadewijk A, Lomas DA, Stolk J, Marciniak SJ, and Hiemstra PS (2015). Function of monocytes and monocyte-derived macrophages in α1-antitrypsin deficiency. The European respiratory journal 45, 365–376. [PubMed: 25323228]

Vattem KM, and Wek RC (2004). Reinitiation involving upstream ORFs regulates ATF4 mRNA translation in mammalian cells. Proceedings of the National Academy of Sciences of the United States of America 101, 11269–11274. [PubMed: 15277680]

Walter P, and Ron D (2011). The unfolded protein response: from stress pathway to homeostatic regulation. Science (New York, N.Y.) 334, 1081–1086.

Wang M, and Kaufman RJ (2016). Protein misfolding in the endoplasmic reticulum as a conduit to human disease. Nature 529, 326–335. [PubMed: 26791723]

Wang X, and He C (2014). Reading RNA methylation codes through methyl-specific binding proteins. RNA biology 11, 669–672. [PubMed: 24823649]

Wang X, Huang J, Zou T, and Yin P (2017). Human m(6)A writers: Two subunits, 2 roles. RNA biology 14, 300–304. [PubMed: 28121234]

Wei J, Chen L, Li F, Yuan Y, Wang Y, Xia W, Zhang Y, Xu Y, Yang Z, Gao B, et al. (2018a). HRD1-ERAD controls production of the hepatokine FGF21 through CREBH polyubiquitination. EMBO J 37.

Wei J, and Fang D (2021). Endoplasmic Reticulum Stress Signaling and the Pathogenesis of Hepatocarcinoma. International journal of molecular sciences 22.

Wei J, Wei C, Wang M, Qiu X, Li Y, Yuan Y, Jin C, Leng L, Wang J, Yang X, et al. (2014). The GTPase-activating protein GIT2 protects against colitis by negatively regulating Toll-like receptor signaling. Proc Natl Acad Sci U S A 111, 8883–8888. [PubMed: 24879442]

Wei J, Yuan Y, Chen L, Xu Y, Zhang Y, Wang Y, Yang Y, Peek CB, Diebold L, Yang Y, et al. (2018b). ER-associated ubiquitin ligase HRD1 programs liver metabolism by targeting multiple metabolic enzymes. Nature communications 9, 3659.

Wei J, Yuan Y, Jin C, Chen H, Leng L, He F, and Wang J (2012). The ubiquitin ligase TRAF6 negatively regulates the JAK-STAT signaling pathway by binding to STAT3 and mediating its ubiquitination. PLoS One 7, e49567. [PubMed: 23185365]

Weng H, Huang H, Wu H, Qin X, Zhao BS, Dong L, Shi H, Skibbe J, Shen C, Hu C, et al. (2018). METTL14 Inhibits Hematopoietic Stem/Progenitor Differentiation and Promotes Leukemogenesis via mRNA m(6)A Modification. Cell stem cell 22, 191–205.e199. [PubMed: 29290617]

Xiang Y, Laurent B, Hsu CH, Nachtergaele S, Lu Z, Sheng W, Xu C, Chen H, Ouyang J, Wang S, et al. (2017). RNA m(6)A methylation regulates the ultraviolet-induced DNA damage response. Nature 543, 573–576. [PubMed: 28297716]

Xu Y, Melo-Cardenas J, Zhang Y, Gau I, Wei J, Montauti E, Zhang Y, Gao B, Jin H, Sun Z, et al. (2019). The E3 ligase Hrd1 stabilizes Tregs by antagonizing inflammatory cytokine-induced ER stress response. JCI Insight 4.

Xu Y, Zhao F, Qiu Q, Chen K, Wei J, Kong Q, Gao B, Melo-Cardenas J, Zhang B, Zhang J, et al. (2016). The ER membrane-anchored ubiquitin ligase Hrd1 is a positive regulator of T-cell immunity. Nature communications 7, 12073.

Yang H, Qiu Q, Gao B, Kong S, Lin Z, and Fang D (2014). Hrd1-mediated BLIMP-1 ubiquitination promotes dendritic cell MHCII expression for CD4 T cell priming during inflammation. The Journal of experimental medicine 211, 2467–2479. [PubMed: 25366967]

Yang Y, Kong S, Zhang Y, Melo-Cardenas J, Gao B, Zhang Y, Zhang DD, Zhang B, Song J, Thorp E, et al. (2018). The endoplasmic reticulum-resident E3 ubiquitin ligase Hrd1 controls a critical checkpoint in B cell development in mice. J Biol Chem 293, 12934–12944. [PubMed: 29907570]

Yue Y, Liu J, and He C (2015). RNA N6-methyladenosine methylation in post-transcriptional gene expression regulation. Genes & development 29, 1343–1355. [PubMed: 26159994]

Zhang Z, Zhan Q, Eckert M, Zhu A, Chryplewicz A, De Jesus DF, Ren D, Kulkarni RN, Lengyel E, He C, et al. (2019). RADAR: differential analysis of MeRIP-seq data with a random effect model. Genome biology 20, 294. [PubMed: 31870409]

Zhou J, Wan J, Gao X, Zhang X, Jaffrey SR, and Qian SB (2015). Dynamic m(6)A mRNA methylation directs translational control of heat shock response. Nature 526, 591–594. [PubMed: 26458103]

Highlights:

- UPR selectively induces m^6A writer METTL14 protein expression.
- METTL14 suppresses CHOP-induced apoptosis for ER stress adaptation.
- HRD1 is a METTL14 ubiquitin ligase and UPR suppresses HRD1-mediated METTL14 degradation.
- CHOP suppression rescues METTL14-null mice from proteotoxic liver damage.

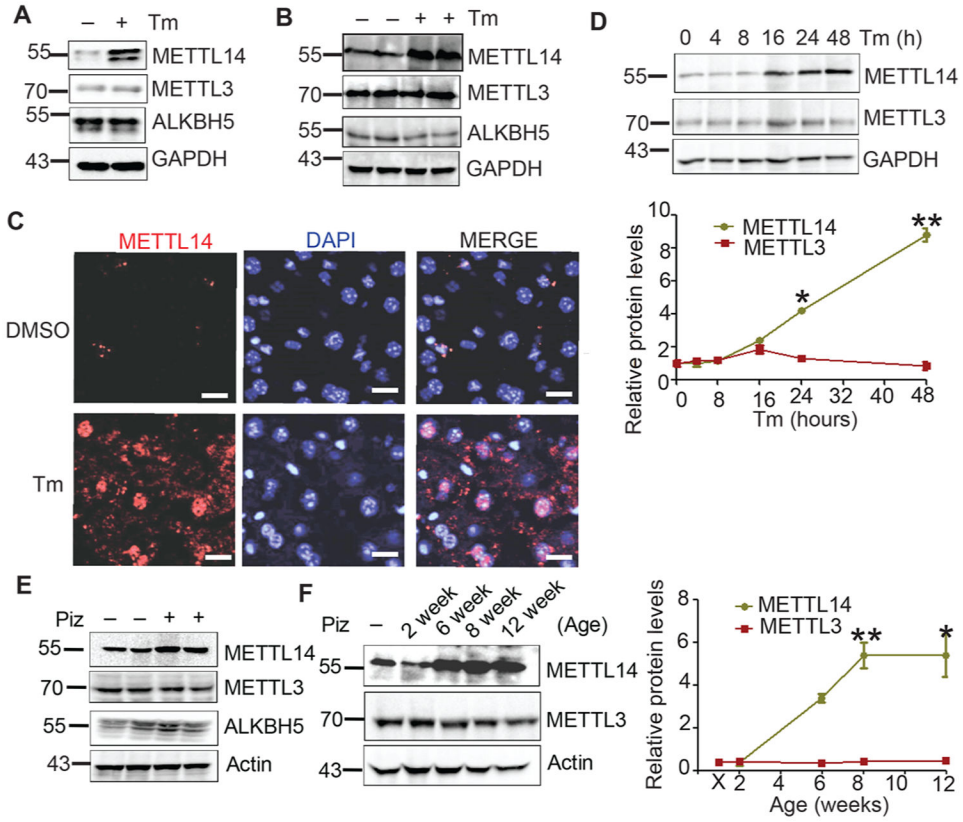

Figure 1: ER stress induces METTL14 protein accumulation.

(A-B) The m^{6}A machinery along with Tm stimulation was measured by immunoblot in HepG2 cells **(A)** and livers **(B)** 24 hours after Tm stimulation. **(C)** Immunofluorescent staining of hepatic METTL14 after 24 hours of Tm stimulation (2 mg/kg). Scale bars: 20 μm. **(D)** METTL14 and METTL3 protein levels were measured after 4-48 hours of Tm stimulation (2 mg/kg). **(E)** Hepatic protein levels of m^{6}A writers METTL3 and METTL14 and eraser ALKBH5 in 6 weeks old WT and PiZ mouse livers were measured by immunoblot. **(F)** Western blotting for METTL3 and METTL14 in livers of 2-12 weeks of age. The band analysis tools of ImageLab software version 4.1 (Bio-Rad) were used to select and determine the background-subtracted density of the bands in all the blots. The relative protein was normalized with GAPDH or Actin expression. Quantification data in (D) & (F) are from three independent experiments (N=3).

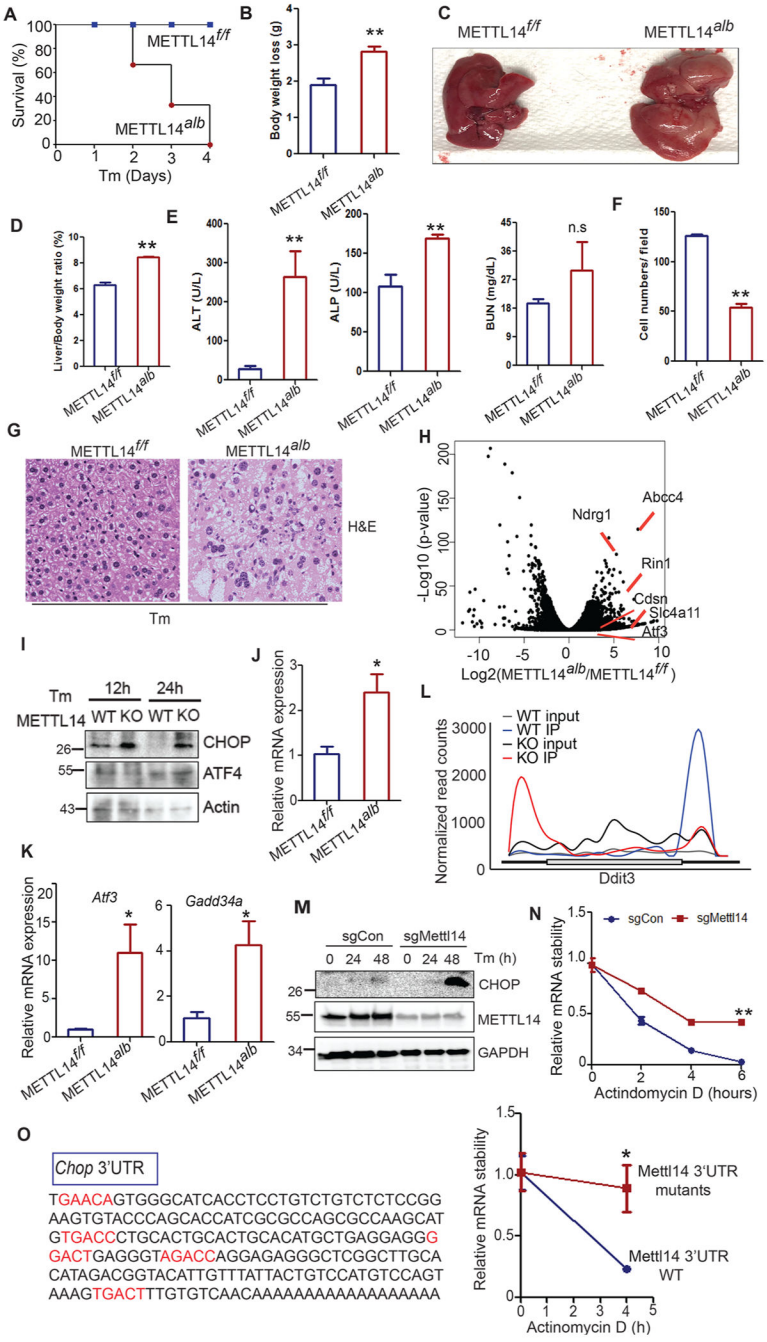

Figure 2: METTL14 protected the mice from ER-stress induced liver damage.

(A) Survival rates of METTL14$^{f/f}$ and METTL14^{alb} mice after challenged with Tm (1mg/kg, n=6 per group). **(B)** Body weight loss 24 hours after Tm administration of the male mice, (n=6 per group). **(C)** Morphology of the liver from **(B). (D)** Liver weight and body weight ratio from METTL14$^{f/f}$ and METTL14^{Alb} challenged with Tm (1mg/kg) for 24 hours, (n=6 per group). **(E)** Serum ALT, ALP and BUN levels from the serum of METTL14$^{f/f}$ and METTL14^{Alb} mice challenged with Tm (1mg/kg) for 24 hours, (n=6 per group). **(F-G)** H&E stain and hepatocytes numbers of the liver from **(B). (H)** Volcano plot

of the genes from WT and METTL14^{alb} livers 24h after Tm injection, (n=3 per group). **(I)** Western blot analysis of CHOP and ATF4 from WT and METTL14^{alb} livers 12h and 24h after Tm injection. **(J-K)** Relative hepatic *Chop, Atf3* and *Gadd34* mRNA in WT and METTL14^{alb} mice from **(H).** The expression values were normalized to those that were obtained with the control *actb* (encoding beta-actin). **(L)** Metagene profiles of m^{6}A distribution across the CHOP mRNA in METTL14$^{f/f}$ and METTL14^{Alb} mouse livers. **(M)** CHOP protein in WT and METTL14^{cas9} NIH3T3 cells 24/48 hours after Tm (100ng/ml) stimulation. **(N)** *Chop* mRNA levels were measured by qPCR in WT and METTL14^{cas9} NIH3T3 cells treated with Tm (250ng/ml) for 12 hours and Actinomycin D (1 μg/ml) for the indicated times. **(O)** The potential m^{6}A methylation sites in the *Chop* mRNA 3'UTR from bioinformatics prediction are shown in red (left). The stability of WT and mutate *Chop* mRNA in transfected NIH3T3 cells was determined (right). The data are representative of three independent experiments (mean ± SEM) *: P<0.05. **: P<0.01.

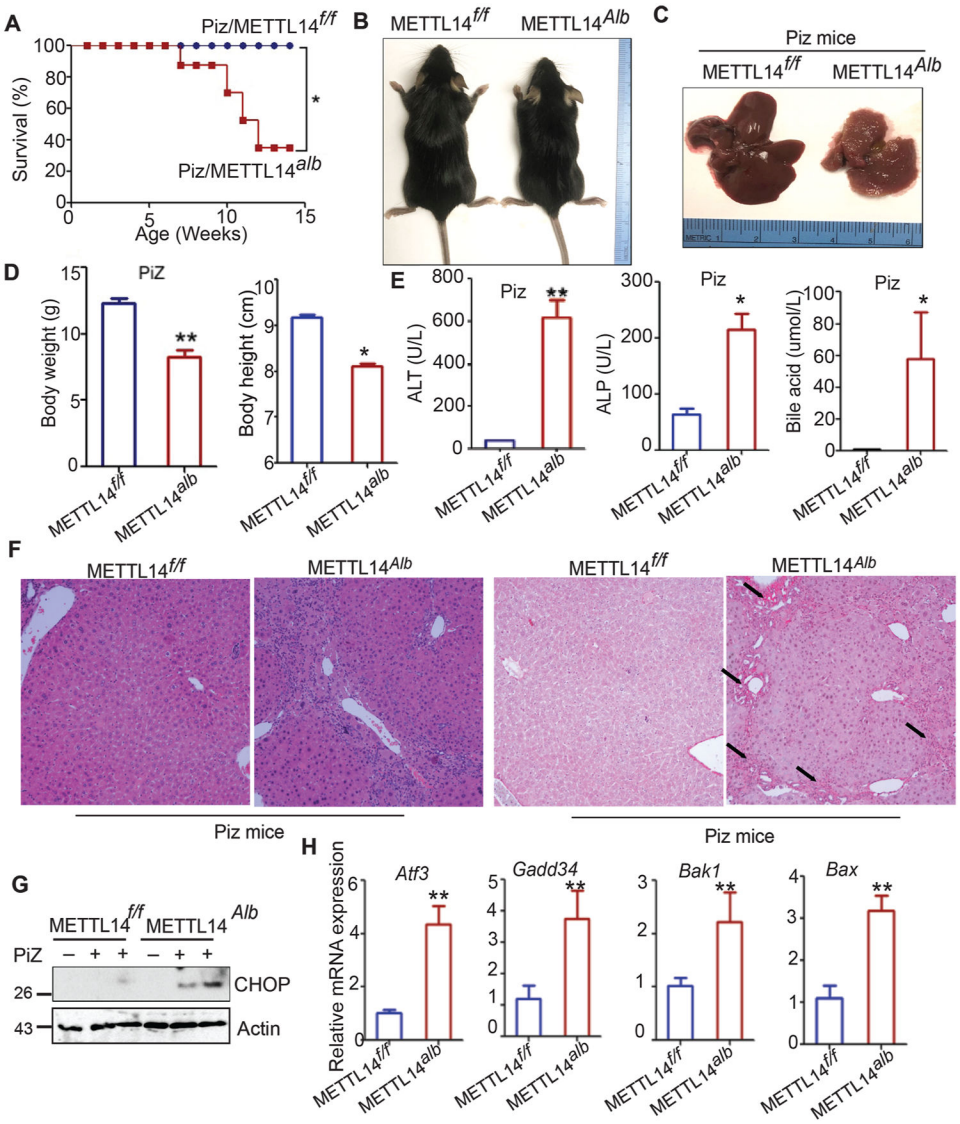

Figure 3: METTL14 ablation aggravates chronic proteotoxic stress induced liver damage.

(A) Survival rates of PiZ/METTL14$^{f/f}$ and PiZ/METTL14^{Alb} male mice. **(B)** Representative full body image of PiZ/METTL14$^{f/f}$ and PiZ/METTL14^{Alb} male mice. **(C)** Morphology of the liver from PiZ/METTL14$^{f/f}$ and PiZ/METTL14^{Alb} male mice. **(D)** Body weight and body heights of PiZ/METTL14$^{f/f}$ and PiZ/METTL14^{Alb} male mice at the age of 6 weeks. **(E)** Serum ALT, ALP and bile acid levels from **(D)**. **(F)** H&E stain and Sirtus Red stain of the liver from **(B)**. **(G)** Western blot analysis of CHOP from PiZ/METTL14$^{f/f}$ and Piz/METTL14^{alb} livers at the age of 6 weeks. **(H)** Hepatic *Atf3, Gadd34, Bak1* and *Bax* mRNA from PiZ/METTL14$^{f/f}$ and Piz/METTL14^{alb} livers (n=4 per group). The Expression values were normalized to those that were obtained with the control *actb* (encoding beta-actin). The data are representative of three independent experiments (mean ± SEM) *: P<0.05. **: P<0.01.

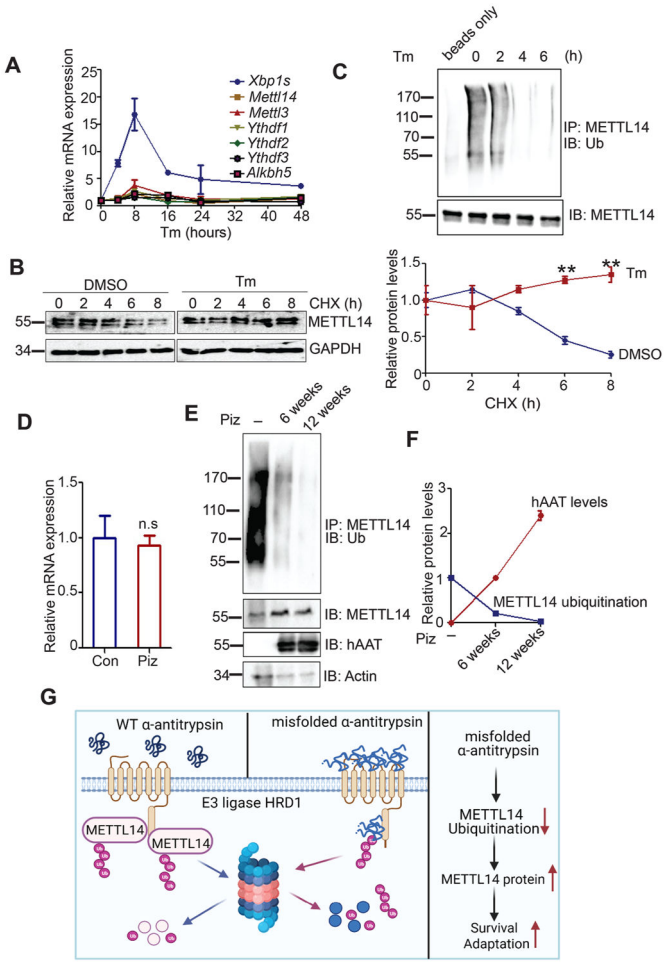

Figure 4: ER stress upregulates METTL14 at the post-translational level.

(A) The mRNA levels of genes encoding m^{6}A machinery along with Tm stimulation were measured by qPCR. **(B)** HepG2 cells were pretreated with Tm (2 μg/ml) for 6 hours. METTL14 protein levels were analyzed after translation inhibitor cycloheximide (CHX, 50 μg/ml) stimulation. **(C)** METTL14 ubiquitination in Tm pre-treated (1ug/ml) HepG2 cells by immunoprecipitation with (lanes 2-5) or without (beads only, lane 1) anti-METTL14 Abs (top panel). METTL14 protein levels in the whole cell lysates were analyzed as a loading control (bottom panel). **(D)** Relative *Mettl14* mRNA levels from WT and Piz livers at the age of 6 weeks old. The Expression values were normalized to those that were obtained with the control *actb* (encoding beta-actin). **(E-F)** The ubiquitination of METTL14 in the livers of WT, 6 weeks and 12 weeks old Piz mice. **(G)** Model for unfolded protein regulation of HRD1-mediated METTL14 ubiquitination and degradation under WT and AAT accumulation conditions. The protein semi-quantification in B & F was analyzed by ImageLab software version 4.1 (Bio-Rad) as the background-subtracted density (N=3).

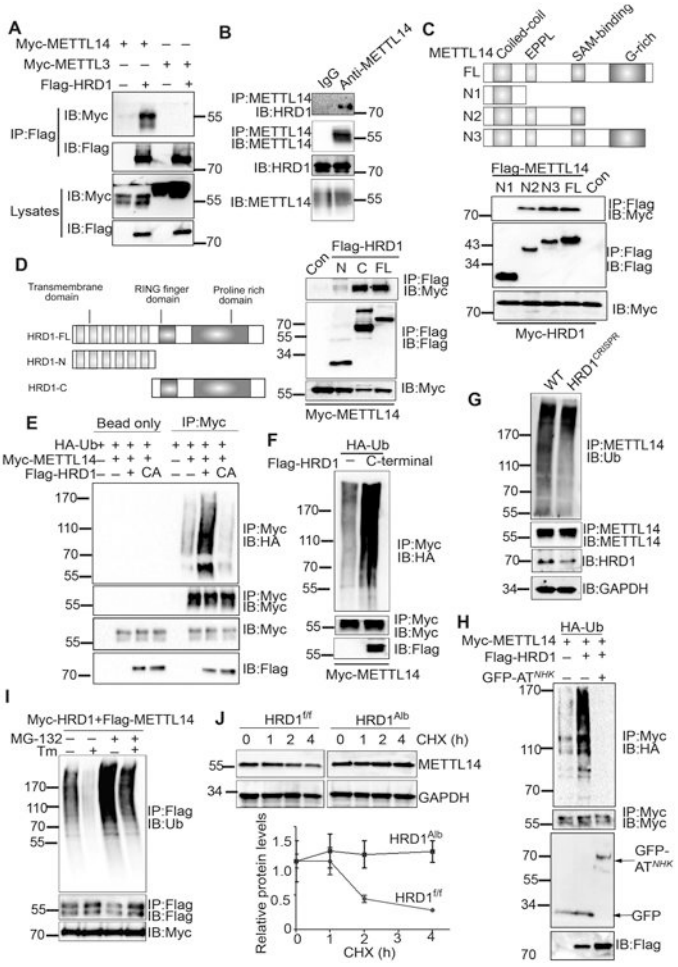

Figure 5: HRD1 is the E3 ligase of METTL14.

(A) The interaction between METTL14 or METTL3 with HRD1 in transfected 293T cells. **(B)** The endogenous interaction between METTL14 and HRD1 in HepG2 cells. **(C)** Interactions of full-length and truncates of METTL14 with HRD1. **(D)** Interactions of full-length HRD1, N-terminal HRD1 and C-terminal HRD1 with METTL14. **(E)** The ubiquitinated METTL14 in transiently transfected HEK293T cells by immunoprecipitation with (lanes 5-4) or without (beads only, lanes 1-4) anti-Myc Abs (top panel). The same membrane was reprobed by anti-Myc (2nd panel), the METTL14 (3rd panel) and HRD1 (bottom panel) protein levels in the whole cell lysates were analyzed as loading controls. **(F)** Analysis of the ubiquitinated METTL14 in C-terminal HRD1 transfected 293T cells. **(G)** Analysis of ubiquitination of endogenous METTL14 in WT and HRD1^{cas9} HepG2 cells. **(H)** Immunoblot analysis of the ubiquitinated METTL14 after IP of Myc-agarose METTL14 after Flag-HRD1 and misfolded antitrypsin null Hong Kong (AT^{NHK}) expression. **(I)** Myc-HRD1 and Flag-METTL14 were transfected to the 293T cells. 48 hours after transfection, the transfected 293T cells were incubated with Tm and MG132 for indicated time. Immunoblot analysis of the endogenous ubiquitination of METTL14 after IP of Flag-agarose in transfected 293T cells. **(J)** Immunoblot analysis of METTL14 protein stability in WT and HRD1 LKO primary hepatocytes. The protein semi-quantification in B & F was

analyzed by ImageLab software version 4.1 (Bio-Rad) as the background-subtracted density (N=4).

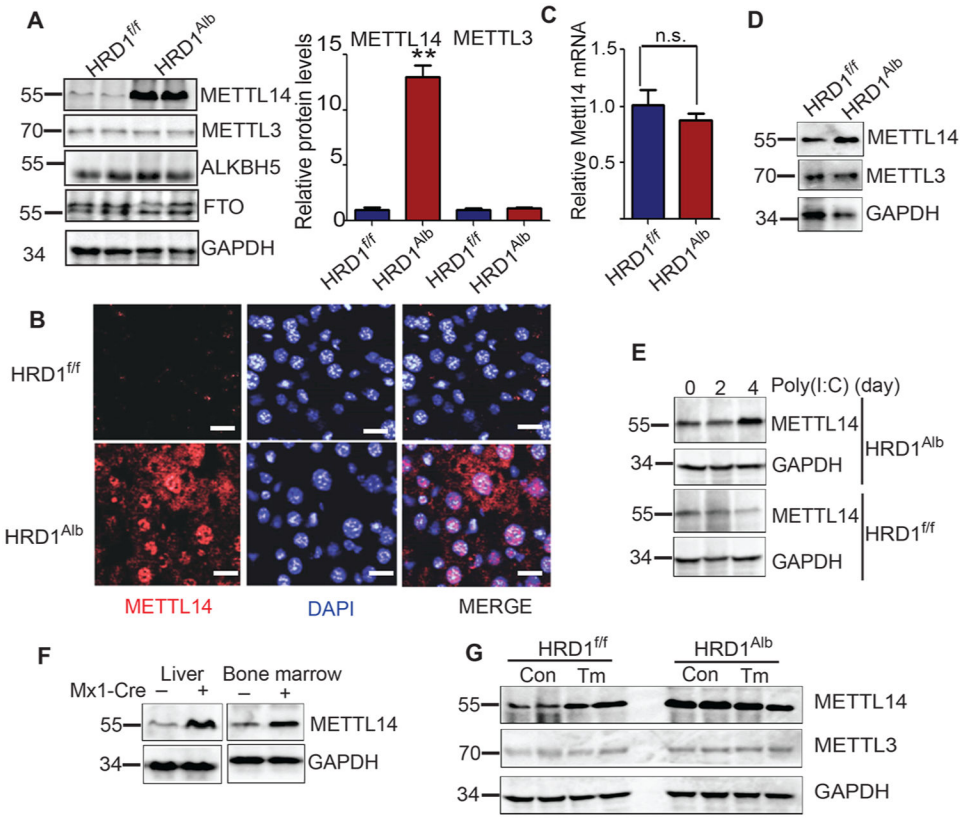

Figure 6: HRD1-deficiency in hepatocytes induces METTL14 levels.

(A) Hepatic protein levels of m6A writer (METTL14 and METTL3) and eraser proteins (ALKBH5 and FTO) in *HRD1*$^{f/f}$ and *HRD1*^{Alb} livers were measured by immunoblot. Values, mean ± SEM; **, p<0.01 by Student's t test. **(B)** Immunofluorescent staining of hepatic METTL14 in *HRD1*$^{f/f}$ and *HRD1*^{Alb} mice. **(C)** Relative METTL14 mRNA from *HRD1*$^{f/f}$ and *HRD1*^{Alb} livers were measured by qPCR. The Expression values were normalized to those that were obtained with the control *actb* (encoding beta-actin). **(D)** METTL14 and METTL3 protein levels in *HRD1*$^{f/f}$ and *HRD1*^{Alb} primary hepatocytes were measured by immunoblot. **(E)** Hepatic protein levels of METTL14 from WT and polyI:C injected HRD1$^{f/f}$Mx1-Cre^{+} mice were measured by immunoblot. **(F)** Hepatic and Bone marrow derived protein levels of METTL14 from WT and polyI:C injected HRD1$^{f/f}$Mx1-Cre^{+} mice were measured by immunoblot. **(G)** Hepatic protein levels of METTL14 and METTL3 from WT and Tm stimulated *HRD1*$^{f/f}$ and *HRD1*^{Alb} mice were measured by immunoblot.

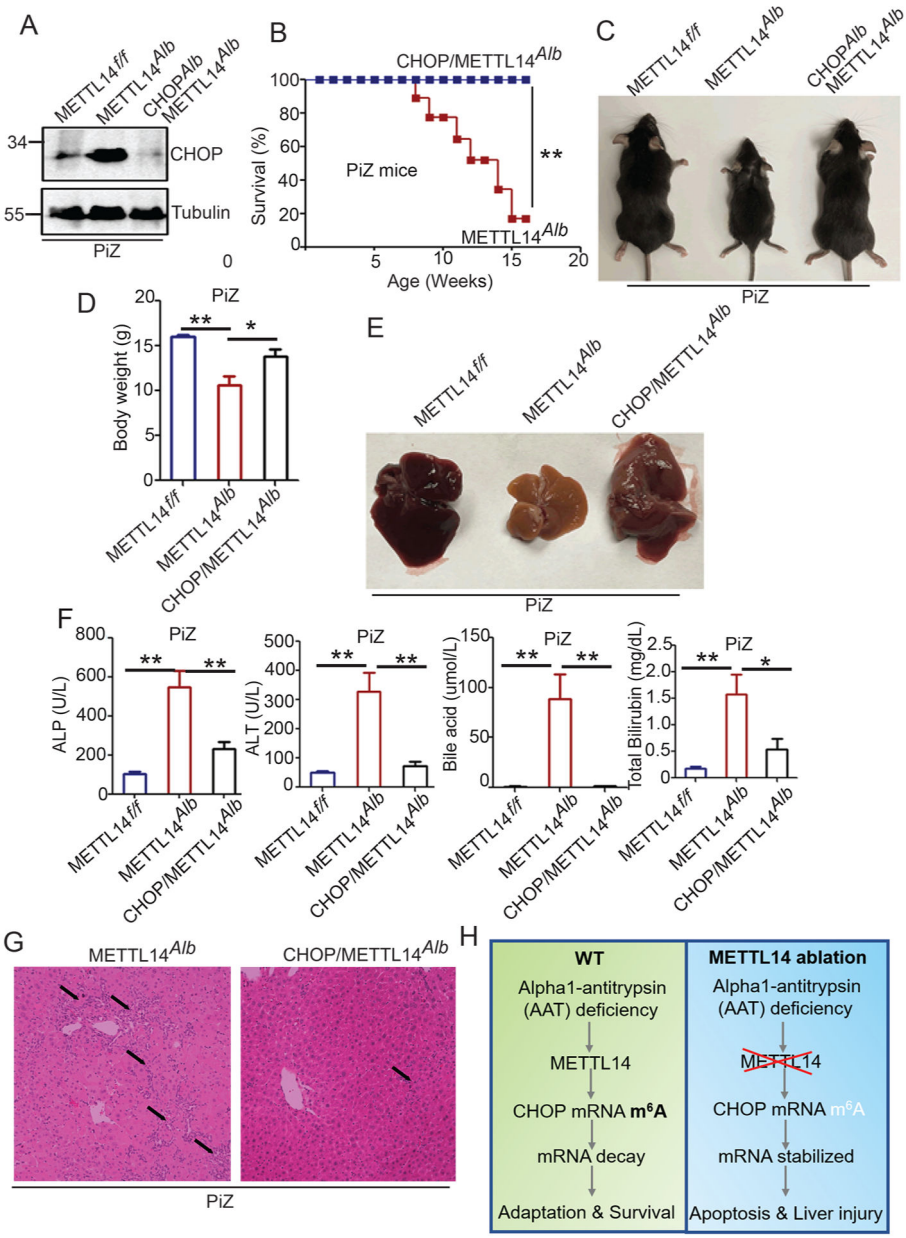

Figure 7: METTL14 protects AAZ-induced liver injury through suppressing CHOP protein expression.

(A) Immunoblot analysis of CHOP protein from PiZ/METTL14$^{f/f}$, PiZ/METTL14^{Alb} and PiZ/METTL14^{Alb}CHOP^{Alb} livers. **(B)** Survival rates of PiZ/METTL14^{Alb} and PiZ/METTL14^{Alb}CHOP^{Alb} male mice, (n=16 per group). **(C)** Gross morphology of the PiZ/METTL14$^{f/f}$, PiZ/METTL14^{Alb} and PiZ/METTL14^{Ab}/CHOP^{Alb} male mice. **(D)** Body weight and liver and body weight ratio of PiZ/METTL14$^{f/f}$ and PiZ/METTL14^{Alb} male mice at the age of 6 weeks, (n=4 per group). **(E)** Gross morphology of the liver from **(D)**. **(F)** Serum ALT, ALP, bile acid and total bilirubin levels from (**D**). The data are representative of three independent experiments (mean ± SEM) *: P<0.05. **: P<0.01. **(G)** H&E stain of the

liver from PiZ/METTL14$^{f/f}$, PiZ/METTL14^{Alb} and PiZ/METTL14^{Alb}/CHOP^{Alb} male mice. **(H)** A working model how METTL14 protects liver from AATD induced liver injury.

KEY RESOURCES TABLE

REAGENTS or RESOURCES	SOURCE	IDENTIFIER
Antibodies		
Anti-METTL14	Abcam	Cat# ab98166; RRID:AB_10672570
Anti-METTL3	Abcam	Cat# ab195352; RRID:AB_2721254
Anti-ALKBH5	Abcam	Cat# ab195377; RRID:AB_2827986
Anti-FTO	Abcam	Cat# ab124892; RRID:AB_10972698
Anti-human AAT	Abcam	Cat# ab207303;
Anti-ACTIN	Sigma	Cat# A2103; RRID:AB_476694
Anti-GAPDH	Cell Signaling	Cat# 2118S; RRID:AB_561053
Anti-CHOP	Cell Signaling	Cat# 5554S; RRID:AB_10694399
Anti-ATF4	Cell Signaling	Cat# 11815S; RRID:AB_2616025
Anti-Ubiquitin	Cell Signaling	Cat# 3933S; RRID:AB_2180538
Anti-Myc	Santa Cruz	Cat# Sc-40; RRID:AB_2857941
Anti-Flag	Sigma	Cat# F-1804; RRID:AB_262044
Anti-HRD1	Sigma	Cat# HPA024300; RRID:AB_1851073
Anti-HA	Santa Cruz	Cat# Sc-7392; RRID:AB_627809
Anti-GFP	Santa Crez	Cat# Sc-8334; RRID:AB_641123
Anti-Tubulin	Proteintech	Cat# 10094; RRID:AB_2210695
Goat Anti-Rabbit IgG Antibody (H+L), Peroxidase	Millipore	Cat# 401353; RRID:AB_437794
Bacterial and virus strains		
DH5alpha Chemically Competent Cells (High Efficiency)	NEB	Cat# C2987H
DH5alpha Chemically Competent Cells (Subcloning Efficiency)	NEB	Cat# C2988J
Stbl3 Chemically Competent Cells	Invitrogen	Cat# C737303
Chemicals, peptides, and recombinant proteins		
Nitrocellulose Blotting Membrane	GE	Cat#45004002
Protein G Sepharose 4 Fast Flow resin	GE	Cat# GE17-0618-02
SuperSignal West Pico PLUS Chemiluminescent Substrate	Thermo	Cat# 34577
SuperSignal West Dura Extended Duration Substrate	Thermo	Cat# 34076
SuperSignal West Femto Maximum Sensitivity Substrate	Thermo	Cat# 34095
Tunicamycin	Tocris	Cat# 351610
Poly(I:C)	Sigma	Cat# 31852-29-6
Cycloheximide	Sigma	Cat# C7698
Actinomycin D	Millipore	Cat# 50-76-0
MG-132	Sigma	Cat# M7449
Q5 HiFi DNA Polymerase	New England Biolabs	Cat# M0491
T4 DNA ligase	New England Biolabs	Cat# M2622S
Complete proteinase inhibitor cocktail	Roche	Cat# 11697498001
Protein G Magnetic Beads	New England Biolabs	Cat# S1430S
Protein G Agarose	Thermo Scientific	Cat# 15920010
Lipofectamine 3000	Invitrogen	Cat# L3000001

REAGENTS or RESOURCES	SOURCE	IDENTIFIER
10X RIPA buffer	Millipore	Cat# 20-188
Collagenase type I	Worthington Biochemical	Cat# LS004194
Critical commercial assays		
qScript cDNA Synthesis Kit	Quanta	Cat# 95047
PerfeCTa SYBR Green SuperMix for iQ	Quanta	Cat# 95053
Epimark N^6-methyladenosine enrichment kit	NEB	Cat# E1610S
TruSeq Stranded mRNA Sample Prep Kit	Illumina	Cat# 20020594
Dynabeads mRNA purification kit	Thermo	Cat# 61006
GenElute mRNA kit	Sigma	Cat# MRN10
RNeasy Mini Kit	QIAGEN	Cat# 74004
Q5 Site-Directed Mutagenesis Kit	New England Biolabs	Cat# E0554S
Deposited data		
RNA sequencing datasets	This manuscript	https://www.ncbi.nlm.nih.gov/geo/query/acc.cgi?acc=GSE185109
Original western blot images and Microscopy data	Mendeley	https://data.mendeley.com/datasets/cnn3hhztjm/1
Experimental models: Cell lines		
Human: HepG2	ATCC	Cat# HB-8065
Human: 293T	ATCC	Cat# CRL-3216
Mouse: NIH 3T3	ATCC	Cat# CRL-1658
Experimental models: Organisms/strains		
Mouse: NOD.Cg-Prkdcscid Il2rgtm1Wjl Tg(SERPINA1*E342K)#Slcw/SzJ	The Jackson Laboratory	Cat# 028842
Mouse: METTL14fl/fl: B6	Weng et al., 2018	N/A
Mouse: HRD1fl/fl: B6	Yang et al., 2014	N/A
Mouse: B6.FVB(129)-Tg(Alb1-cre)1Dlr/J	The Jackson Laboratory	Cat# 016832
Mouse: B6.Cg-Tg(Mx1-cre)1Cgn/J	The Jackson Laboratory	Cat# 003556
Mouse: B6.Cg-Ddit3tm1.1Irt/J	The Jackson Laboratory	Cat# 030816
Oligonucleotides		
Primers for qPCR, see the primer table below	This paper	N/A
sgRNA targeting sequence: mouse METTL14: ACATCCCTGATGAAATTCTG	This paper	N/A
sgRNA targeting sequence: human HRD1: CCGCCATCATCACTGCCGTG	This paper	N/A
Recombinant DNA		
lentiCRISPR v2	Addgene	Cat# 52961
Plasmid: pcDNA3/Flag-METTL14	Addgene	Cat #53740
Plasmid: pCMV/Myc-HRD1	Xu et al., 2016	N/A
Plasmid: pCMV/Myc-METTL14	This paper	N/A
Plasmid: pCMV/Myc-METTL3	This paper	N/A
Plasmid: pCMV/Flag-HRD1	Xu et al., 2016	N/A
Plasmid: pCMV/Flag-HRD1^{CA}	Xu et al., 2016	N/A
Plasmid: HA-Ub	Xu et al., 2016	N/A
Plasmid: GFP-AT^{NHK}	Sun et al., 2015	N/A

REAGENTS or RESOURCES	SOURCE	IDENTIFIER
Plasmid: AT^{WT}	Addgene	Cat #24527
Plasmid: pCMV/Flag-HRD1N	Wei et al., 2018a	N/A
Plasmid: pCMV/Flag-HRD1C	Wei et al., 2018a	N/A
Plasmid: pCMV/Flag-METTL14N1	This paper	N/A
Plasmid: pCMV/Flag-METTL14N2	This paper	N/A
Plasmid: pCMV/Flag-METTL14N3	This paper	N/A
Software and algorithms		
HISAT2 (version 2.1.0)	Kim et al., 2015	http://daehwankimlab.github.io/hisat2/
RADAR	Zhang et al., 2019	https://github.com/scottzijiezhang/RADAR
ImageLab	BioRad	https://www.bio-rad.com/en-us/product/image-lab-software?ID=KRE6P5E8Z
DESeq2 (version 1.18.1)		https://bioconductor.org/packages/release/bioc/html/DESeq2.html
PANTHER in 2013	Mi et al., 2013	http://www.pantherdb.org/
Gene set enrichment analysis	Subramanian et al., 2005	https://www.gsea-msigdb.org/gsea/index.jsp
Others		
ChemiDoc MP imaging system	BioRad	https://www.bio-rad.com/en-us/sku/12003154-chemidoc-mp-imaging-system?ID=12003154
Illumina HiSeq4000	Illumina	https://www.illumina.com/systems/sequencing-platforms/hiseq-3000-4000.html
RP-HPLC (C18 column)	Agilent	https://www.agilent.com/en/product/small-molecule-columns/reversed-phase-hplc-columns
Sciex 6500+ triple-quadrupole LC mass spectrometer	SCIEX	https://sciex.com/products/mass-spectrometers/triple-quad-systems/triple-quad-6500plus-system